ISSN 0016-7029, Geochemistry International, 2006, Vol. 44, No. 1, pp. 19–32. © Pleiades Publishing, Inc., 2006.
Original Russian Text © V.S. Urusov, V.B. Dudnikova, E.V. Zharikov, 2006, published in Geokhimiya, 2006, No. 1, pp. 23–37.

Crystal Chemical and Energy Analysis of Partition Coefficients of Impurities during Melt Crystallization: The Case of Olivine

V. S. Urusov[1, 2], V. B. Dudnikova[1], and E. V. Zharikov[3, 4]

[1]*Vernadsky Institute of Geochemistry and Analytical Chemistry, Russian Academy of Sciences, ul. Kosygina 19, Moscow, 119991 Russia*

[2]*Geological Faculty, Moscow State University, Vorob'evy gory, Moscow, 119899 Russia*

[3]*General Physics Institute, Russian Academy of Sciences, ul. Vavilova 38 D, Moscow, 119991 Russia*

[4]*Mendeleev University of Chemical Technology, Miusskaya pl. 9, Moscow, 125047 Russia*

Received May 12, 2005

Abstract—Partition coefficients (K) between forsterite crystal and melt are experimentally determined for many univalent, bivalent, trivalent, and tetravalent trace elements. Using numerical modeling, we calculated the energies of intrinsic and impurity defects in forsterite (E_{df}) and the energies of dissolution of univalent, bivalent, trivalent, and tetravalent impurities (E_{ds}). These results are compared with literature data. A linear dependence is established for the energy of defects on the charge of the impurity ion and the relative difference in the radii of the impurity and matrix ions $\Delta r/d$, where d is the average interatomic distance in the matrix. Partition coefficients are described by parabolic dependences on $\Delta r/d$ and charge of the impurity ion using literature data on K of impurity elements in olivines and impurity ion dissolution energies. Linear dependences $-RT\ln K - (\Delta r/d)^2$ and $E_{ds} - (\Delta r/d)^2$ pass through the origin for isovalent substitutions and are well apart from it for heterovalent substitutions. Linear dependence $(\Delta r/d)^2$ has a free term of about 200 kJ/mol, which is approximately equal to a half of the energy of formation of the Frenkel defect in forsterite; this defect maintains electroneutrality. If valency is compensated due to addition into the melt of an ion with another charge (than that of the impurity ion), $E_{ds} - (\Delta r/d)^2$ and $-RT\ln K - (\Delta r/d)^2$ lines at low $(\Delta r/d)^2$ shift to the origin. This means that energy consumption for coupled isomorphism is lower than that for the formation of intrinsic structural defects. Correlation dependences are proposed for the distribution of impurities and the energy of their dissolution. They indicate the increasing contribution of the entropy components of impurity ion dissolution energy during heterovalent isomorphism.

DOI: 10.1134/S0016702906010046

INTRODUCTION

Replenishment of data on distribution of chemical elements between crystal and melt is very important for understanding the nature of element fractionation during crystallization, controlling impurity doping process, and obtaining materials with desired properties. Experimental studies and geochemical observations demonstrate that the partition coefficient of an element (K) depends on the size and charge of its ion, temperature, pressure, compositions of crystals and melts, and oxygen fugacity during crystallization for elements with variable valency. In some cases, the interpretation of experimental results requires consideration of the real character of chemical bonds in crystals.

Experimental determination of partition coefficients is normally a laborious procedure because it is related to the analysis of compositional changes in crystal and melt during crystallization [1]. Thermodynamic calculations of K values were successfully used in many studies devoted to the crystallization of alkali halogenides (e.g., [1, 2]) and in investigations of some oxide and silicate systems [1]. However, they require knowledge of excess functions of mixing of components (enthalpy and entropy of mixing) in solid and liquid phases. Experimental studies in this area provide only scarce data. This gap can be partially filled using crystal chemical method for estimating the enthalpy of mixing [1, 3].

Methods of numerical modeling of crystal structures are extensively developed and allow calculations of the energy of impurity ion dissolution (E_{ds}) [4]. Transition from E_{ds} values to K estimation is difficult because the effects of temperature, defect concentrations in crystals, entropy contribution to free energy of their dissolution, and melt properties should be taken into account. Calculations of K values using methods of molecular thermodynamics are theoretically the strictest [5]. However, this approach also has some constraints and unresolved problems.

The above problems highlight the importance of correlation methods in K estimation. They allow us to classify the collected materials, predict unknown K values, and correct data deviated from general dependences. Correlations of K values with the maximum solubility of the impurity component in the crystal phase, the standard electrode potential of the impurity component, the melting temperature of the impurity,

the energy of the crystal lattice of the impurity component, and the diffusion coefficient of the impurity ion in the crystal matrix were determined for some systems [2, 6]. There is a significant empirical correlation between K and the difference in radii (Δr) of the impurity and matrix ions. Onuma *et al.* [7] suggested describing experimental data with a parabolic dependence of $\ln K$ on the radius of the impurity ion. Such a dependence was also verified later for some inorganic compounds and minerals [1, 4, 8–18]. Theoretical analysis [1, 12] leads to the conclusion that K values should be a function of the relative difference of the impurity and host ion radii, $\Delta r/d$ (where d is the interatomic distance in the matrix crystal). Experimental data on partition coefficients can be also presented using dependences on Δr^3 (difference in the atomic volumes of the ions participating in the substitution) [19].

In this study, we experimentally determined the partition coefficients of various impurities between forsterite (*Fo*) crystal and melt and analyzed their dependences on the difference in ionic radii and charges. These data are compared with the results of numerical modeling of intrinsic and impurity defects in *Fo* to reveal the relation between macroscopic properties, which can be determined experimentally, and calculated energy of impurity ion dissolution.

EXPERIMENTAL DETERMINATION OF PARTITION COEFFICIENTS OF IMPURITY BETWEEN FORSTERITE CRYSTAL AND MELT

Forsterite single crystals were grown from melt (T_{melt} = 1890°C) using Czochralski's technique. The starting material was prepared of ultrapure SiO_2 and MgO taken in stoichiometric proportion. Impurities were added as oxides and carbonates. Crystals were grown in inert atmosphere from iridium crucible on a single crystal *Fo* seed, which was oriented along [010] (*Pnma* orientation). For V and Cr as elements with variable valency, crystallization was performed under various redox conditions, and oxygen fugacity varied within $-4 \le \log(f_{O_2}) \le -0.9$. Crystal rotation rate was 12–20 r/min. Crystallization rate was 2 mm/h in most runs and was increased to 7 mm/h in some cases for estimation of the influence of the crystallization rate on K value. The cooling rate of the crystals was about 100 K/h. Proportion of the crystallized melt normally did not exceed 5–10%.

Concentrations of impurities in the crystals were determined using electron microprobe analysis (EMPA), neutron activation (NAA), inductively coupled plasma atomic emission spectroscopy (ICP-AES), atomic absorption (AA), and flame atomic emission spectroscopy (FAES).

The partition coefficient was estimated by extrapolation of the dependence $K(g) = C_S/C_{Lo}$ to $g = 0$, where C_S is the impurity content in crystal, C_{Lo} is the initial impurity content in the melt, and g is the proportion of the crystallized melt. Note that changes in growth rate did not lead to significant differences in partition coefficients.

Results of K determination are shown in Table 1. Some data were published earlier [11, 20]. Table 1 also lists the radii of the impurity ions (r) for six- and fourfold coordinations (for tetravalent impurities) [21], the initial impurity contents in the melt (C_{Lo}), the partition coefficients (K), the confidence level of their determination (ΔK), and the method of impurity analysis in the crystal.

The partition coefficient for V (K_V) is 0.07 and does not change with variations of oxygen fugacities. Invariable K_V values are caused by the fact that the main part of vanadium within the studied interval of oxygen fugacities occurs in V^{4+} form [22]. However, K_{Cr} changes from 0.18 to 0.09 and is 0.18 at $f_{O_2} = 10^{-4}$ for crystals with dominant Cr^{3+} [23]. Titanium in crystals grown in inert atmosphere generally occurs in Ti^{4+} form [24].

The experimentally obtained K values are presented in Fig. 1 as function of difference in radii of impurity and matrix cations (Δr) with allowance for bivalent and trivalent ion substitution for Mg in octahedral sites of forsterite and tetravalent ion substitution for Si in tetrahedral sites.

Comparison of our results with data of [25] demonstrates that K of trivalent impurities in [25] are overestimated in most cases relative to our data (Fig. 1), probably due to the addition of Na^+ ions to the melt in [25], which could compensate valency.

FORMATION AND INTERACTION OF DEFECTS IN THE SYSTEM OF FORSTERITE CRYSTAL AND MELT

Forsterite structure (Fig. 2) consists of isolated zigzag chains of Mg octahedra parallel to b axis (space group *Pnma*) with M1 octahedra in the chain axes and M2 octahedra at the chain tips. Within one layer in the ab plane, the chains of Mg octahedra alternate with similar chains of octahedral vacancies with M3 vacancies at their axes and M4 vacancies at their tips. The next layer of Mg octahedra is shifted relative to the previous one so that the filled Mg chains lie above the vacancy chain of the previous layer and *vice versa* [26]. The chains of filled octahedra of the first and third layers are linked with Si tetrahedra S1 and separated by tetrahedral vacancies S2 and S3.

Impurity ion dissolution in crystal can be considered as exchange reactions between crystal phase and melt containing the main and impurity components in forms of ionic oxides. Isovalent substitutions of Mg ion by bivalent impurity Me^{2+} can be written as the following quasichemical reaction:[1]

[1] Hereafter, the Kroeger notations are used: subscript index denotes site in crystal, the superscript corresponds to excess positive charge (●) or excess negative charge (') of the impurity ion relative to the charge of matrix ion (×), v is vacancy, and I is interstice.

Table 1. Coefficients of impurity partitioning between forsterite crystal and melt

Impurity	r (Å)	C_{L0}, wt %	K	ΔK	Analytical method
Univalent impurities					
Li	0.76	0.2	0.007	0.001	ICP-AES, FAES
Bivalent impurities					
Ni	0.69	0.8–3.3	0.75	0.04	EMPA
Co	0.745	0.18–0.2	0.53	0.04	EMPA
Mn	0.83	1.0	0.39	0.02	EMPA
Ca	1.0	1.12	0.073	0.005	EMPA
Sr	1.18	1.22	0.0007	0.0002	AA
Ba	1.35	1.44–1.91	0.0004	0.0002	ICP-AES
Trivalent impurities					
Cr	0.615	0.14	0.18	0.018	EMPA
Ga	0.62	4.4×10^{-4}	0.055	0.009	NAA
Sc	0.745	2.8×10^{-4}	0.19	0.02	NAA
Lu	0.861	1×10^{-3}	0.1	0.01	NAA
Er	0.89	0.4–0.6	0.02	0.002	EMPA
Gd	0.938	4.9×10^{-3}	0.022	0.003	NAA
Eu	0.947	9.4×10^{-4}	0.0054	0.0009	NAA
Sm	0.958	1×10^{-3}	0.007	0.001	NAA
Nd	0.983	0.17–0.19	0.002	0.0005	NAA
La	1.032	8×10^{-4}	0.002	0.0007	NAA
Tetravalent impurities					
Ti	0.42	0.34–0.67	0.06	0.003	ICP-AES, EMPA
V	0.46	0.35–2	0.07	0.005	EMPA
Hf	0.58	1.25	0.0017	0.0008	NAA
Zr	0.59	0.65–1.26	0.002	0.0008	ICP-AES, NAA

$$Mg^{\times}_{Mg} + (MeO)_L \Leftrightarrow Me^{\times}_{Mg} + (MgO)_L, \quad (1)$$

where subscript L means that the corresponding oxides are components of the melt.

The analogous reaction for a tetravalent impurity Me^{4+} in Si site can be written as:

$$Si^{\times}_{Si} + (MeO_2)_L \Leftrightarrow Me^{\times}_{Si} + (SiO_2)_L. \quad (2)$$

The energy of impurity ion dissolution E_{ds} for reactions (1) and (2) can be calculated by Eqs. (3) and (4):

$$E_{ds}(Me^{2+}) = E_{df}(Me^{\times}_{Mg}) + E_{lat}(MgO) - E_{lat}(MeO), \quad (3)$$

$$E_{ds}(Me^{4+}) = E_{df}(Me^{\times}_{Si}) + E_{lat}(SiO_2) - E_{lat}(MeO_2), \quad (4)$$

where E_{df} is the energy of impurity defects ($Me^{\times}_{Mg}$ or $Me^{\times}_{Si}$) in *Fo*, and E_{lat} is the energy of lattices of pure oxides. The small difference in the enthalpies of oxide melting can be neglected in this approximation.

The heterovalent substitution of Mg^{2+} by univalent Me^{+} or trivalent Me^{3+} ions produces an impurity defect with excess negative or positive charge. Various mechanisms of charge compensation of such defect are possible. The excess negative charge induced by a univalent impurity ion can be compensated at the expense of intrinsic *Fo* defects (vacancies in oxygen sites $v^{\cdot\cdot}_O$ and interstitial Mg incorporation $Mg^{\cdot\cdot}_I$) in the following ways:

$$\frac{1}{2}(Me_2O)_L + Mg^{\times}_{Mg} + \frac{1}{2}O^{\times}_O \Leftrightarrow Me'_{Mg} + \frac{1}{2}v^{\cdot\cdot}_O + (MgO)_L, \quad (5)$$

$$\frac{1}{2}(Me_2O)_L + Mg^{\times}_{Mg} \Leftrightarrow Me'_{Mg} + \frac{1}{2}Mg^{\cdot\cdot}_I + \frac{1}{2}(MgO)_L. \quad (6)$$

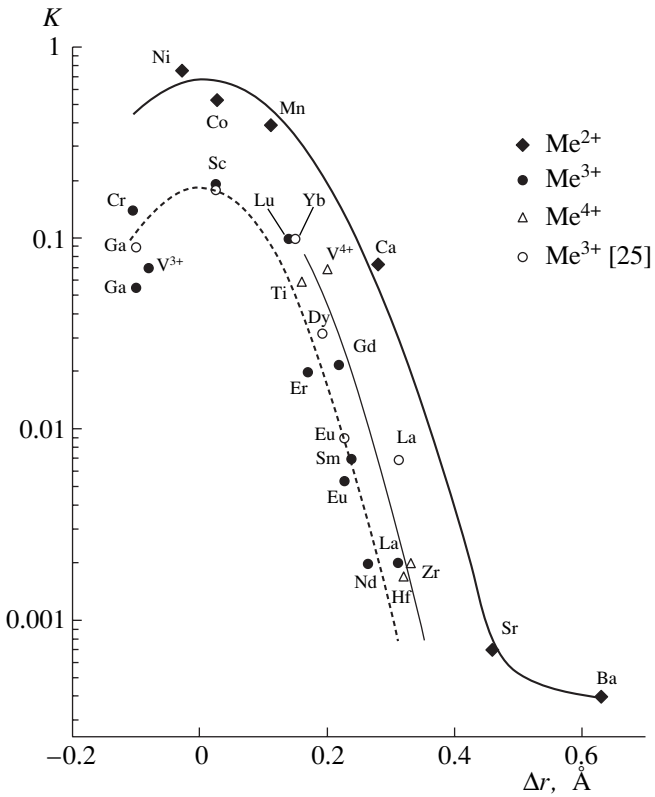

Fig. 1. Coefficients of impurity partitioning between forsterite crystal and melt as functions of difference in radii of ions participating in substitution (Onuma curves).

Compensation of excess charge for the trivalent impurities can occur by the following mechanism:

$$\frac{1}{2}(Me_2O_3)_L + \frac{3}{2}Mg_{Mg}^{\times} \Leftrightarrow Me_{Mg}^{\cdot} + \frac{1}{2}v_{Mg}'' + \frac{3}{2}(MgO)_L, \quad (7)$$

where v_{Mg}'' is vacancy in Mg site. Charge compensation can also occur with coupled incorporation of trivalent and univalent ions[2] in Mg site:

$$\frac{1}{2}(Me_2O_3)_L + \frac{1}{2}(M_2O)_L + 2Mg_{Mg}^{\times} \Leftrightarrow M_{Mg}' + Me_{Mg}^{\cdot} + 2(MgO)_L, \quad (8)$$

as well as a pair of trivalent ions in Mg and Si sites:

$$\frac{1}{2}(Me_2O_3)_L + \frac{1}{2}(M_2O_3)_L + 2Mg_{Mg}^{\times} + Si_{Si}^{\times} \Leftrightarrow M_{Si}' + Me_{Mg}^{\cdot} + 2(MgO)_L + (SiO_2)_L. \quad (9)$$

[2] One of the ions is denoted by M instead of Me to distinguish impurity ions in Eqs. (8), (9), and (16).

The energies of dissolution for reactions (5)–(9) are described by the following equations:

$$E_{ds}(Me^{+}) = E_{df}(Me_{Mg}') + \frac{1}{2}E_{df}(v_O^{\cdot\cdot}) + E_{lat}(MgO) - \frac{1}{2}E_{lat}(Me_2O), \quad (10)$$

$$E_{ds}(Me^{+}) = E_{df}(Me_{Mg}') + \frac{1}{2}E_{df}(Mg_I^{\cdot\cdot}) + E_{lat}(MgO) - \frac{1}{2}E_{lat}(Me_2O), \quad (11)$$

$$E_{ds}(Me^{3+}) = E_{df}(Me_{Mg}^{\cdot}) + \frac{1}{2}E_{df}(v_{Mg}'') + \frac{3}{2}E_{lat}(MgO) - \frac{1}{2}E_{lat}(Me_2O_3), \quad (12)$$

$$E_{ds}(Me^{3+}, M^{+}) = E_{df}(Me_{Mg}^{\cdot}) + E_{df}(M_{Mg}') + 2E_{lat}(MgO) - \frac{1}{2}E_{lat}(Me_2O_3) - \frac{1}{2}E_{lat}(M_2O), \quad (13)$$

$$E_{ds}(Me^{3+}, M^{3+}) = E_{df}(Me_{Mg}^{\cdot}) + E_{df}(M_{Si}') + 2E_{lat}(MgO) + 2E_{lat}(SiO_2) - \frac{1}{2}E_{lat}(Me_2O_3) - \frac{1}{2}E_{lat}(M_2O_3). \quad (14)$$

It is known that charged defects can form dual, triple, and more complex associates:

$$2Me_{Mg}^{\cdot} + v_{Mg}'' \Leftrightarrow (Me_{Mg}v_{Mg}Me_{Mg})^{\times}, \quad (15)$$

$$Me_{Mg}^{\cdot} + M_{Mg}' \Leftrightarrow (Me_{Mg}M_{Mg})^{\times}. \quad (16)$$

In these cases, the energy of the associate formation from isolated defects should be taken into account in the dissolution energy calculation.

NUMERICAL MODELING OF DEFECTS IN FORSTERITE CRYSTALS

Numerical modeling can be used for estimation of defect energies and calculation of the energy of the optimized structural model of crystal. The energy of the defect depends on its interaction with the surrounding matrix and is determined by the minimization of the static energy of the crystal with this defect during changes in the position of atoms and dipole moments around the point defect. This energy presents the difference between the energy of a crystal distorted by defect formation and the energy of a defect-free crystal.

According to the Mott-Littleton model, a crystal can be divided into two regions: region I, containing a defect and its surroundings; and region II, the rest of the crystal. Shifts and dipole moments in the inner region I

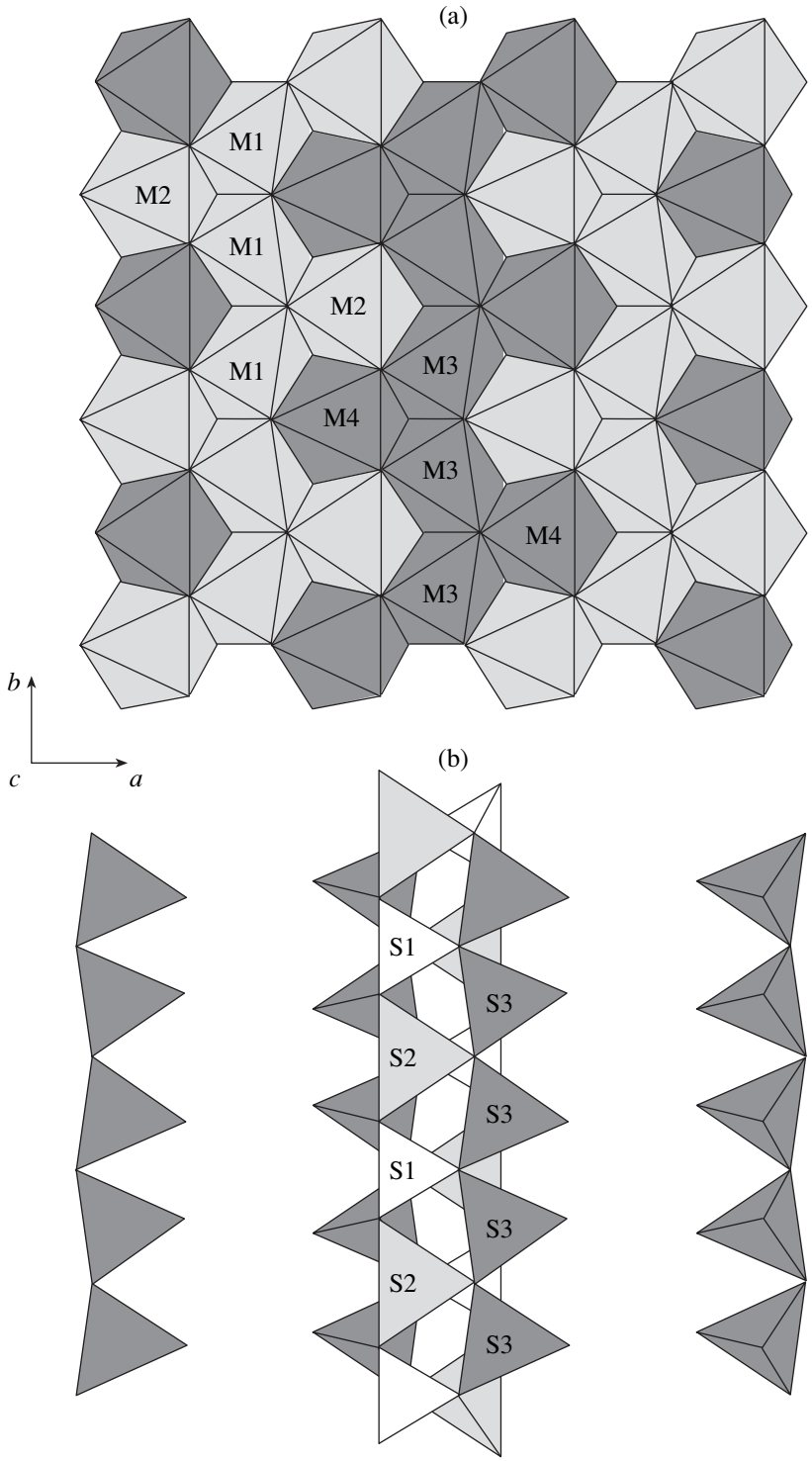

Fig. 2. Forsterite structure: (a) occupied (M1, M2) and vacant (M3, M4) octahedral sites; (b) occupied (S1) and vacant (S2, S3) tetrahedral sites.

are determined by consideration of ion interaction, while the crystal in the outer region II is regarded as a dielectric medium in continuum approximation. Calculation was performed in static approximation for the case of infinite dilution. The region I was 10 Å in radius and included 638 ions or >90 molecular units (about 20 unit cells).

Modeling of *Fo* structure was performed using GULP (General Utility Lattice Program) [27] in frames of ionic approximation. The pair potential U_{ij} of inter-

Table 2. Intrinsic defects in forsterite crystal and their energies

Defect	Site	E_{df}, kJ/mol
v''_{Mg}	M1	**2360**
	M2	2550
$Mg_I^{\cdot\cdot}$	M3	–1110
	M4	**–1650**
v''''_{Mg}	S1	9960
$Si_I^{\cdot\cdot\cdot\cdot}$	S2	–7490
	S3	**–7620**
$v_O^{\cdot\cdot}$	O1	2700
	O2	2430
	O3	**2350**
Frenkel magnesium defect		E_F = 360
Schottky defect		E_{Sch} = 570

action of ions i and j with charges q_i and q_j is an algebraic sum of several terms:

$$U_{ij}(R_{ij}) = q_i q_j e^2/R_{ij} + B_{ij}\exp(-R_{ij}/\lambda_{ij}) - c_{ij}/R_{ij}^6. \quad (17)$$

The first term presents Coulomb interaction, the second one, repulsion originating due to overlap of the electron shells of neighboring atoms, while the last describes Van der Waals interaction; R_{ij} is interatomic distance, B_{ij}, λ_{ij}, and c_{ij} are parameters of short-range potentials.

It is known that chemical bonds in such oxide and silicate compounds as Mg_2SiO_4 cannot be adequately described using ionic model proper. One of the efficient methods to account for the covalent component is to consider the polarizability of individual atoms, usually of anions. The polarizability of an oxygen ion is normally taken into account using a shell model. In this approach, the ion is regarded as a core, which includes the whole mass and is surrounded by a spherical charged shell modeling a valent electron cloud. The core and shell are linked by the harmonic elastic constant χ_i:

$$U_i^S = (1/2)\chi_i l_i^2, \quad (18)$$

where l_i is the distance between the core and the center of the shifted shell.

Three-particle interaction was considered for the directed partially covalent *ijk* bond O–Si–O using the potential of the bond bend:

$$U_{ijk} = (1/2)\alpha_{ijk}(\theta_{ijk} - \theta_0)^2, \quad (19)$$

where α_{ijk} is constant, θ_{ijk} is the equilibrium angle between bonds, θ_0 is the angle in a regular tetrahedron (109.47°). The values of the parameters of interaction potentials were taken from [28–30].

The results of modeling the structure of defect-free *Fo* crystal can be compared with experimental data [31]: deviation of calculated values from experimental ones is <1% for unit cell parameters and 1.5% for volume. The largest difference in atomic coordinates is 5%; the difference in bulk modules is 12%.

The results of the calculation of the energy of the intrinsic defects in *Fo* are given in Table 2. The lowest values of defect energies are given in bold; the corresponding defects are the most energetically favorable and, hence, should be most abundant.

The M1 site is more preferential for Mg vacancies than the M2 site. Oxygen vacancies more readily form in site O3, while the O1 site with short bond Si–O1 is the least favorable. Energies of Mg (v''_{Mg}) and O ($v_O^{\cdot\cdot}$) vacancies are almost equal, whereas the formation of Si vacancies ($v_{Si}^{\cdot\cdot\cdot\cdot}$) requires fourfold energy consumption. Like for the oxygen interstices, the probability of $v_{Si}^{\cdot\cdot\cdot\cdot}$ formation is lower as compared to the other defects of *Fo* [32].

The energy of formation of Frenkel defects for Mg ions $0 \Leftrightarrow v''_{Mg} + Mg_I^{\cdot\cdot}$ per one particle can be estimated using the following equation:

$$E_F = \frac{1}{2}[E_{df}(v''_{Mg}) + E_{df}(Mg_I^{\cdot\cdot})]. \quad (20)$$

E_F is about 360 kJ/mol (Table 4).

The energy of formation of Schottky defects per one particle of Mg_2SiO_4 molecule can be derived from

$$E_{Sch} = \frac{1}{7}[(2E_{df}(v''_{Mg}) + E_{df}(v_{Si}^{\cdot\cdot\cdot\cdot}) + 4E_{df}(v_O^{\cdot\cdot}) - E_{lat}(Mg_2SiO_4)]. \quad (21)$$

It is about 570 kJ/mol. Therefore, Frenkel defects form significantly more easily in *Fo* structure then Schottky defects. The energies of intrinsic defects listed in Table 2 are consistent with experimental data and other calculation results [33, 34].

The values used of parameters of interaction potentials Me-O for impurity centers and obtained energies of defects (E_{df}) and energies of impurity ion dissolution (E_{ds}) are listed in Table 3. The table also presents energies of pure impurity oxide lattices (E_{lat}). The energies of MgO and SiO_2 lattices are not given in Table 3 and are equal to –3980 and –12 390 kJ/mol, respectively. The energies of pure oxide lattices and the energies of the corresponding defects in forsterite were calculated at the same repulsion parameters. Since the energies of defect formation are the differences between these values, we can expect compensation of errors originated, for instance, due to the use of ionic approximation.

The data of Table 3 for the most bivalent impurities well agree with calculation results [35]. The largest dif-

Table 3. Parameters of potentials and results of calculation of energies of impurity defects (E_{df}) and energies of impurity dissolution (E_{ds}) in forsterite

Impurity	Δ*r*, A	Parameters of potentials		Calculated energies, kJ/mol				
				E_{df}		E_{lat}	E_{ds}	
		B, kJ/mol	λ, Å	M1	M2	Me_iO_y	M1	M2
Univalent impurities								
Li^+	0.04	292.3	0.3472	**1621**	1679	–2808	**208**	266
Na^+	0.3	611.1	0.3535	**1900**	1930	–2402	**285**	314
K^+	0.66	902.8	0.3698	**2248**	2258	–2142	**502**	512
Rb^+	0.8	1010.8	0.3793	2431	**2430**	–2045	637	**636**
Bivalent impurities								
Ni^{2+}	–0.03	1582.5	0.2882	**–33**	–30	–4012	**–5**	–2
Co^{2+}	0.025	14991.7	0.2951	35	**31**	–3940	–10	**–14**
Fe^{2+}	0.06	1207.6	0.3084	101	**91**	–3871	–12	**–22**
Mn^{2+}	0.11	1007.4	0.3262	241	**218**	–3737	–6	**–29**
Ca^{2+}	0.28	1090.4	0.3437	570	**516**	–3469	55	**1**
Sr^{2+}	0.46	959.1	0.3721	924	**843**	–3224	164	**84**
Ba^{2+}	0.63	905.7	0.3976	1306	**1203**	–2959	281	**178**
Ttrivalent impurities								
Cr^{3+}	–0.105	1255.2	0.349	–1489	**–1609**	–13202	310	**191**
Ti^{3+}	–0.05	1715.7	0.3069	–2208	**–2277**	–14509	245	**175**
Sc^{3+}	0.025	1299.4	0.3312	–1912	**–2001**	–13941	256	**167**
Yb^{3+}	0.148	1309.6	0.3462	–1502	**–1621**	–13197	294	**175**
Y^{3+}	0.18	1345.1	0.3491	–1388	**–1514**	–13002	311	**185**
Gd^{3+}	0.218	1336.8	0.3551	–1237	**–1374**	–12753	337	**200**
Eu^{3+}	0.227	1358	0.3556	–1201	**–1340**	–12695	344	**205**
Nd^{3+}	0.263	1379.9	0.3601	–1059	**–1206**	–12469	374	**226**
Pu^{3+}	0.28	1376.2	0.3593	–1084	**–1230**	–12509	369	**222**
Tetravalent impurities								
Ge^{4+}	0.13	1035.5	0.3464	887		–11489	–43	
Ti^{4+}	0.16	754.2	0.3879	1665		–10851	98	
V^{4+}	0.2*	706.882	0.3865	1339		–11055	–25	
Hf^{4+}	0.32	1454.6	0.35	2155		–10554	290	
Zr^{4+}	0.33	1608.1	0.3509	2465		–10446	492	
Ce^{4+}	0.52*	1986.8	0.3511	2982		–10061	623	
U^{4+}	0.55*	2246.8	0.3554	3418		–9706	705	
Th^{4+}	0.6*	2201.1	0.357	3430		–9686	698	

Note: Asterisks – ionic radii obtained by extrapolating the dependence of *r* on the coordination number.

ferences in E_{ds} values of 40 and 80 kJ/mol for Sr and Ba impurities are caused by using different values of repulsion parameters. The results of our calculations for heterovalent substitutions cannot be compared with the results of [36] because E_{df} values are presented in [36] only graphically, while E_{ds} values for the case of charge compensation by intrinsic defects are not reported. However, note the significant difference in E_{df} values for Cr^{3+}. The difference may also be related to the use of different parameters for repulsion potentials. The problem of selection of these parameters is unresolved at present.

As follows from analysis of calculation results, the univalent impurities (except for large Rb^+ ion) probably prefer the M1 site to the M2 site.

The energies of dissolution in both octahedral sites are close for bivalent Ni, Co, and Fe; E_{ds} for Ni^{2+} is

Table 4. Calculated energies of dissolution (kJ/mol) of trivalent impurities in the mode of impurity-vacancy associates and by mechanism of coupled isomorphism with valency compensating ion

Me	Associates		Compensator		
	E_{df}	E_{ds}	Li'_{Mg}	Na'_{Mg}	Al'_{Si}
Cr^{3+}	–1119	65	49	126	342
Ti^{3+}	–2461	48	34	111	327
Sc^{3+}	–1901	43	26	103	319
Yb^{3+}	–1148	48	34	111	327
Y^{3+}	–936	56	43	121	337
Gd^{3+}	–656	72	59	136	352
Eu^{3+}	–589	77	64	141	357
Nd^{3+}	–318	99	85	162	378
Pu^{3+}	–368	94	81	158	374

somewhat lower in the M1 site, while E_{ds} for Co^{2+} and Fe^{2+} is some lower in the M2 site. According to experimental data [37], these ions can replace Mg in both the M1 and M2 sites, but they (particularly, Ni^{2+}) prefer the M1 site. In natural olivines, Fe^{2+} contents can prevail in the M1 or M2 sites, depending on the conditions of olivine formation, and Fe^{2+} distribution between M1 and M2 can be modified by heating under conditions of controlled oxygen fugacity [38]. The energies of dissolution of the other impurities are lower for the M2 site than for the M1 site, which is consistent with experimental data on the prevalent substitution of Mg in M2 by Ca^{2+} and Mn^{2+} [37, 39, 40].

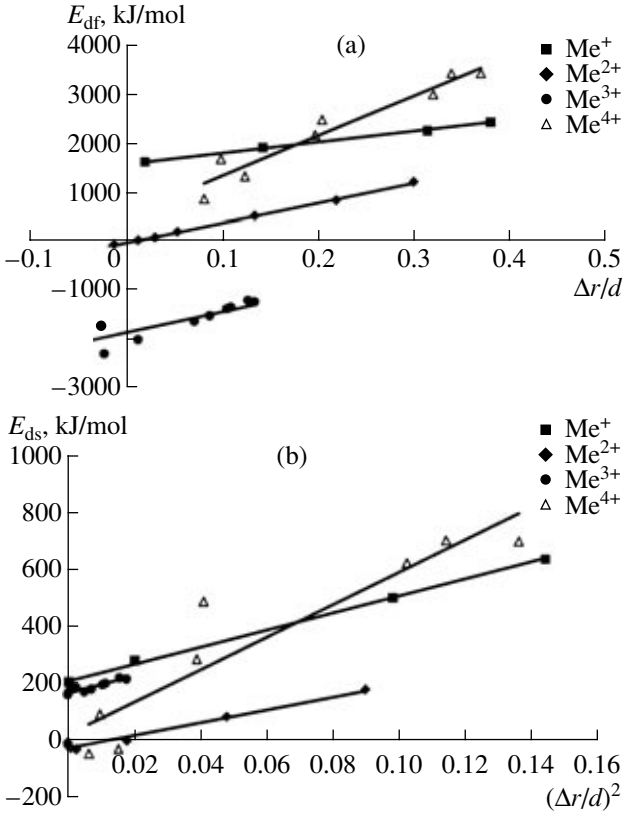

Fig. 3. Dependence of the energy of impurity defects (E_{df}) on the size parameter $\Delta r/d$ (a) and the energy of impurity dissolution in forsterite crystal (E_{ds}) on $(\Delta r/d)^2$ (b).

According to theoretical calculations, trivalent impurities should prefer the M2 site. These conclusions agree with EPR data indicating that Gd^{3+} occupy the M2 site in *Fo* [41]. However, analysis of EPR spectra shows that Cr^{3+} is preferentially incorporated into the M1 site [42–45]. The Cr^{3+} ions replace Mg ions in *Fo* in the M1 and M2 sites in proportion varying from 3 : 2 [43] to 9 : 2 [42] with this ratio growing under more oxidized conditions.

Thus, with the above assumptions, calculation of the energies of impurity ion dissolution in some cases allows the correct estimation of ion distribution between sites. These estimates, however, are not always successful because cation distribution is governed by various factors. This distribution depends not only on cation size, its charge, and electronegativity, strength of crystal field, and nature of site in crystal structure, but varies also with temperature, rate of crystal cooling, and oxygen fugacity. The chemical bonding of an element in different structural sites and the energies of stabilization of transitional element atoms by the crystal field in sites with different symmetries should be taken into account to estimate the energy of site ordering [12]. These factors cannot be properly considered in numerical modeling.

DEPENDENCE OF ENERGIES OF DEFECTS AND ENERGIES OF IMPURITY DISSOLUTION ON SIZE AND CHARGE OF IMPURITY ION

Figure 3 shows the dependence of the energy of defect (Fig. 3a) and energy of impurity ion dissolution (Fig. 3b) on the relative difference in the radii of the impurity ion and the substituted matrix ion, $(\Delta r/d)$, where d is the average interatomic distance Me-O in the substitution site, which is equal to 2.11 Å for Mg–O and 1.63 Å for Si–O. The energy of defect and energy of impurity dissolution have different values for the M1 and M2 sites. They are represented by their lowest values printed in bold in Table 3.

The energies of defects can be best described by a linear function of the size parameter $\Delta r/d$, while the dissolution energies can be described by a quadratic function.

The dependences of the energies of defects on $\Delta r/d$ can be approximated by the following equations (E_{df} is in kJ/mol):

$$Me^{+}: E_{df} = 2200(70)(\Delta r/d) + 1580(20), \quad R^2 = 1.00;$$

$$Me^{2+}: E_{df} = 3970(70)(\Delta r/d) - 3(11), \quad R^2 = 1.00;$$

$$Me^{3+}: E_{df} = 4300(1200)(\Delta r/d) - 1850(100), \quad R^2 = 0.63;$$

$$Me^{4+}: E_{df} = 8200(800)(\Delta r/d) + 500(200), \quad R^2 = 0.94.$$

Standard uncertainties in the estimation of the coefficients of linear regression are given in parentheses. Correlation coefficients (R^2) are also demonstrated.

The dependences of E_{df} on $\Delta r/d$ for isovalent substitutions ($Me^{\times}_{Mg}$ and $Me^{\times}_{Si}$) pass closer to the origin than those for heterovalent substitutions. Thus, replacement of the host ion with an ion of similar size ($\Delta r/d \longrightarrow 0$) and equal charge only insignificantly changes the total energy of the crystal lattice. These changes can be related to differences in the repulsion parameters of the ions involved in the substitution. These parameters characterize the contribution of the different electron configurations of the impurity ion and the substituted matrix ion. For the heterovalent substitution (Me'_{Mg}, $Me^{\cdot}_{Mg}$), the dependences of the energy of defect on the relative difference in ionic radii cut a segment on the ordinate axis with absolute length of 1500–2000 kJ/mol, i.e., the charged impurity defect causes significant changes in crystal energy, even at small difference in ion sizes. These changes are comparable with changes in *Fo* crystal energies due to intrinsic Mg and O defects (Table 2).

The slope of the dependence of the energy of defect on the relative difference in ionic radii increases in the following sequence: $Me^{+} < Me^{2+} < Me^{3+} < Me^{4+}$; i.e., the energy of defect becomes more sensitive to size incompatibility with increasing charge of the impurity ion. Univalent impurities generally preferring the M1 site have smaller slope of the dependence. Bivalent and trivalent impurities preferring M2 site show a slope about twice as long. The slope of the dependence of E_{df} on $\Delta r/d$ for tetravalent impurities is more than three times larger than for univalent and two times larger than for bivalent impurities. This may indicate that the tetrahedral site is much less elastic than the octahedral one, and the distorted octahedral site M2 is less elastic than the M1 site.

It is known that compressibility is proportional to mole volume for isostructural materials [12, 46–49] or kV = const, where k is bulk module and V is mole volume. Similar dependences were determined for some cation sites in complex crystals [50]. For oxides and silicates, this dependence can be written as

$$k_p d^3/q_c = 7.5 \pm 0.2 \text{ Mbar Å}^3, \quad (22)$$

where k_p is bulk module, d is the average length of the cation–anion bond in a coordination polyhedron, and q_c is the cation charge. The dependence allows estimating k_p value, which is 1.6 ± 0.04 Mbar for MgO_6 octahedron and 6.9 ± 0.2 Mbar for SiO_4 tetrahedron.

The dependences of the energies of impurity dissolution on the square of the relative difference in ionic radii are presented in Fig. 3b and can be described by the following equations (E_{ds} in kJ/mol):

$$Me^{+}: E_{ds} = 3000(80)(\Delta r/d)^2 + 215(7), \quad R^2 = 1.00;$$

$$Me^{2+}: E_{ds} = 2200(150)(\Delta r/d)^2 - 22(6), \quad R^2 = 0.98;$$

$$Me^{3+}: E_{ds} = 3080(400)(\Delta r/d)^2 + 170(4), \quad R^2 = 0.88;$$

$$Me^{4+}: E_{ds} = 5700(900)(\Delta r/d)^2 + 25(70), \quad R^2 = 0.86.$$

For isovalent substitutions ($Me^{\times}_{Mg}(Me^{2+})$, $Me^{\times}_{Si}(Me^{4+})$), and $E_{ds} - (\Delta r/d)^2$, the dependence passes near the origin. For heterovalent substitutions ($Me'_{Mg}(Me^{+})$, $Me^{\cdot}_{Mg}(Me^{3+})$, the corresponding dependences may deviate from the origin by about 200 kJ/mol. This value is comparable with the energy of formation of valency-compensating defects. According to Eqs. (6) and (7), half of the E_F value from Eq. (20), i.e., about 180 kJ/mol, is required for compensation of the excess charge unit of the impurity ion.

The slope of E_{ds} dependence on $(\Delta r/d)^2$ for substitution to the Si site ($Me^{\times}_{Si}(Me^{4+})$) is significantly larger than for substitution to Mg site (Me^{+}, Me^{2+}, and Me^{3+}).

As it follows from phenomenological crystal chemical theory of isomorphous mixing [3, 12], the energy of the dissolution of the isolated impurity can be represented as

$$E_{ds} = m\eta q_c q_a (\Delta r/d)^2,$$

where m is the empirical parameter, which is about 100 kJ/mol for oxides, η is the coordination number in substitution site, q_c and q_a are the formal charges (valencies) of cation and anion. Then, the slope of the $E_{ds} - (\Delta r/d)^2$ dependence will be equal to 2400 kJ/mol for the Mg site and 3200 kJ/mol for the Si site. The former value is close to the average slope for the linear dependences for Me^{+}, Me^{2+}, and Me^{3+} (2700(400) kJ/mol), but the latter is lower than the slope value in the equation Me^{4+} (5700(900) kJ/mol).

The dependence of E_{df} of ionic charge at constant $\Delta r/d$ can be described by a linear function, while the dependence of E_{ds} can be described by a parabola (Fig. 4). Note that E_{df} and E_{ds} shift to higher levels with increasing $\Delta r/d$.

Table 4 also contains estimates of the energy of defect and energy of impurity dissolution for trivalent impurities for the case when defect is impurity–vacancy associate. The sum of the energies of isolated defects in Eq. (12) should be replaced by energy of associate. Comparison of results presented in Tables 3 and 4 demonstrates that the formation of associates is energetically favorable, i.e., impurities should gravitate to intrinsic defects of crystal. This mechanism was proposed by the authors [1, 51] to explain the effect of impurity trapping with abrupt increase of K values for concentrations lower than the concentrations of intrinsic thermal defects of crystal.

Table 4 also includes results of calculation of dissolution energy E_{ds} of trivalent impurities by mechanism of coupled isomorphism, see Eqs. (8) and (9). Note that $E_{ds}(Me^{3+})$ values decrease in the following sequence of valency compensators: $Al'_{Si} > Na'_{Mg} > Li'_{Mg}$. The latter

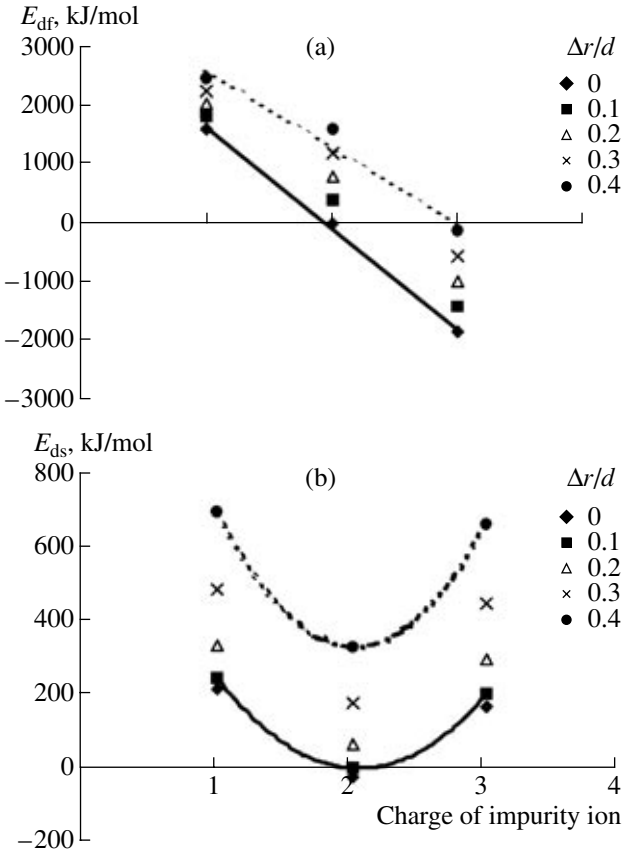

Fig. 4. Dependence of the energy of defects (a) and the energy of impurity dissolution (b) on the charge of impurity ion substituting for Mg^{2+} in forsterite crystal for various $\Delta r/d$ values.

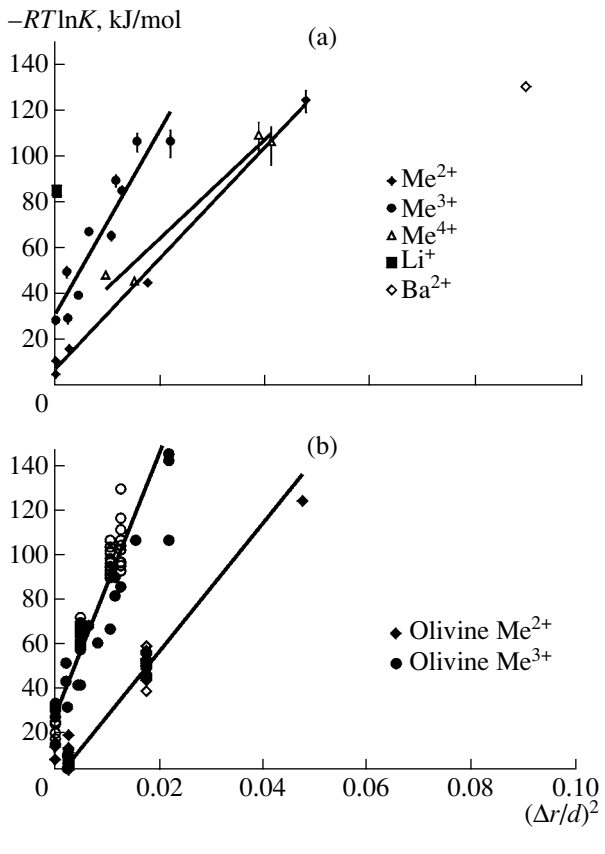

Fig. 5. Correlation of the partition coefficient with squared size parameter for impurities with various valencies in olivine: (a) forsterite melt; (b) silicate melts of various compositions (open symbols denote Fe-bearing olivines).

two dissolution modes are more favorable than the vacancy mechanism of charge compensation. The participation of Li^+ ions in dissolution decreases the energy of Cr^{3+} dissolution by 140 kJ/mol. The formation of $(Me_{Mg}Li_{Mg})^{\times}$ associates gives additional energy saving. For example, E_{ds} decreases by 70 kJ/mol with the formation of $(Cr^{3+}_{M1}Li^{+}_{M1})^{\times}$ associate and by 40 kJ/mol with formation of $(Cr^{3+}_{M2}Li^{+}_{M1})^{\times}$ associate.

CRYSTAL CHEMICAL ANALYSIS OF COEFFICIENTS OF IMPURITY PARTITIONING

Changes in $-RT\ln K$ for ions with equal valencies can be described by linear dependences on $(\Delta r/d)^2$, which are shown in Fig. 5a

Me^{2+}: $-RT\ln K = 2400(100)(\Delta r/d)^2 + 7(2)$, $R^2 = 0.99$;

Me^{3+}: $-RT\ln K = 4000(500)(\Delta r/d)^2 + 32(6)$, $R^2 = 0.88$;

Me^{4+}: $-RT\ln K = 2200(300)(\Delta r/d)^2 + 21(9)$, $R^2 = 0.96$;

where R is absolute gas constant.

K_{Ba} is an exception and has higher values than the values expected from general regularities in K variations with changes of sizes of bivalent ions. This may be related to accuracy in the experimental determination of impurity with low solubility or to the effect of impurity trapping [1, 51]. The probability of the latter mechanism sharply increases for impurities strongly different from matrix ions in properties.

For ions of similar sizes, the coefficient of impurity partitioning between the forsterite crystal and the melt decreases in the following sequence: $Me^{2+} > Me^{4+} > Me^{3+} > Me^{+}$. Lithium with Li^+ radius of 0.76 Å close to the Mg^{2+} radius of 0.72 Å shows the lowest K value as compared to the other cases of heterovalent substitutions. This is consistent with the Goldschmidt rule of isomorphism polarity [12], according to which, the ion with higher charge is more easily incorporated into crystal than the ion with lower charge.

The K values obtained in our experiments of *Fo* crystallization from melt can be compared with literature data [10, 25, 52]. It should be taken into account that forsterite crystals were grown in [25] from melt with addition of Na^+ as charge compensator, while the data of [10] were obtained at temperatures of olivine

crystallization of 1190–1495°C from silicate melts varying in composition from basalt to komatiite. Olivines studied in [52] crystallized at T = 1180–1420°C from synthetic basalts with 5–30 wt % FeO.

Figure 5b shows dependences of $-RT\ln K$ on $(\Delta r/d)^2$, which also involve literature data [10, 25, 52]:

$$Me^{2+}: -RT\ln K = 2990(70)(\Delta r/d)^2 - 5(1),\ R^2 = 0.96;$$

$$Me^{3+}: -RT\ln K = 6000(240)(\Delta r/d)^2 + 24(2),\ R^2 = 0.87.$$

In this case, K_{Ba} values were also excluded from the calculation of the linear correlation. K_{La} values from [10] were also eliminated for the same reason. The plotted lines for Me^{2+} and Me^{3+} differ from the lines that were drawn using only our experimental data. This is probably related to the influence of melt composition.

Figure 6 shows variations of K as a function of the charge of the impurities substituted for Mg. The solid line traces K variation at $\Delta r/d$ = 0.02 and is based on experimental K_{Li} and K values for bi- and trivalent impurities estimated by correlation equations for forsterite. These equations are also used in the calculation of K for bi- and trivalent impurities at $\Delta r/d$ varying from 0.05 to 0.14. Moreover, Fig. 6 shows experimental data for impurities with sizes similar to the Mg^{2+} ion (Li^+, Co^{2+}, and Sc^{3+} with $\Delta r/d \le 0.02$) and for impurities with strongly different sizes (Ca^{2+} and Nd^{3+}, $\Delta r/d$ = 0.13 and 0.12, respectively). Thus, K dependence on impurity ion charge can be described by a parabola. With increasing $\Delta r/d$, the parabola shifts to lowest K values. The parabolic dependence of K on the charge of the impurity ion occupying the M2 site in clinopyroxene was discussed earlier in [53].

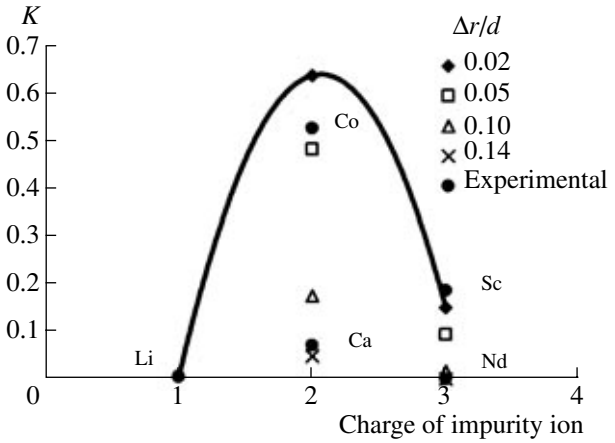

Fig. 6. Dependence of partition coefficient on charge of impurity ion substituted for Mg^{2+} in forsterite crystal for various $\Delta r/d$ values (by correlation equations and experimental data).

THERMODYNAMIC ANALYSIS OF PARTITION COEFFICIENTS OF IMPURITIES

It is known [1] that the coefficient of impurity partitioning between crystal and melt is a function of crystallization temperature (T):

$$-R\ln K_i = [\Delta H^{(S)}_{mix}(i) - \Delta H^{(L)}_{mix}(i) - \Delta H_{melt}(i)]1/T + [\Delta S_{melt}(i) - \Delta S_{vibr}], \quad (23)$$

where $\Delta H^{(S)}_{mix}(i)$ and $\Delta H^{(L)}_{mix}(i)$ are enthalpies of mixing in solid and liquid phases; $\Delta H_{melt}(i)$ and $\Delta S_{melt}(i)$ are enthalpy and entropy of melting of an impurity component; and ΔS_{vibr} is vibration contribution to mixing entropy.

Figure 7a shows temperature dependences of K for some bivalent and trivalent impurities, which are presented as $-R\ln K_i = a_i/T + b_i$. They are obtained using data from [10] and [52]. Coefficients a_i and b_i determined from experimental dependences (Fig. 7a) are enthalpy, $a_i = \Delta H = \Delta H^{(S)}_{mix}(i) - \Delta H^{(L)}_{mix}(i) - \Delta H_{melt}(i)$, and entropy, $b_i = \Delta S = (\Delta S_{melt}(i) - \Delta S_{vibr})$, contributions to the free energy controlling the distribution of impurities.

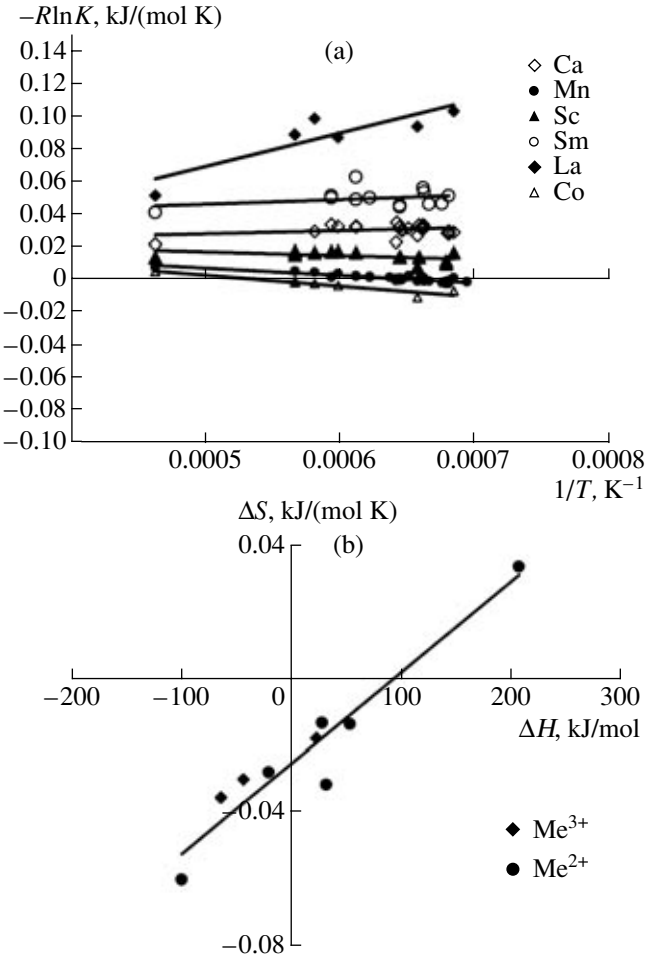

Fig. 7. Dependence of coefficient of impurity partitioning between olivine and silicate melt on crystallization temperature (a) and compensation effect (b).

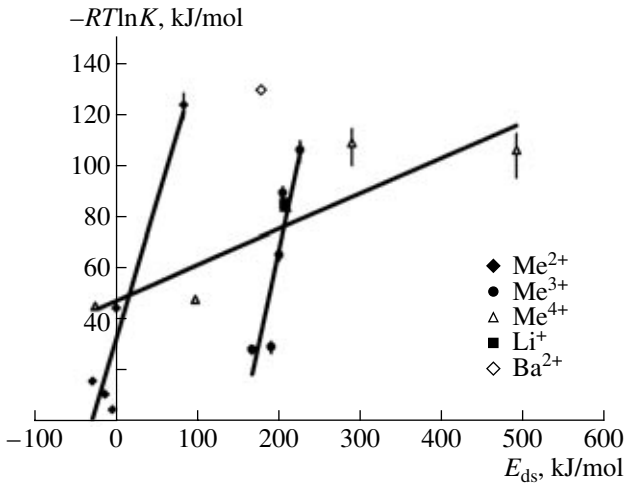

Fig. 8. Correlation between partition coefficients of impurities with various valences and energies of dissolution of these impurities in forsterite crystal.

There is a compensation effect between the entropy and enthalpy components of free energy [3] expressed in a linear correlation between these parameters: $\Delta S = \Delta H/T_{comp}$ + const. Figure 7b verifies the occurrence of such a correlation in our case. It can be presented by the equation $(27 \pm 3) \times 10^{-5}\Delta H - (0.025 \pm 0.003)$ with $R^2 = 0.96$ or $\Delta S = \Delta H/(3700 \pm 500) - 0.02$. Data for bivalent and trivalent impurities are unified within one dependence because calculations demonstrated that differences are within the intervals of experimental uncertainties. The straight line in Fig. 7b does not pass through the origin, which is probably related to the contribution of the enthalpy of the melting of the impurity component. The compensation temperature (T_{comp}) is 3700 ± 500 K, which is close to $T_{comp} \cong 3000$ K for oxide solid solutions [3] and corresponds to the proposed estimate of universal value for $T_{comp} = 3600 \pm 1000$ K [3].

Comparison of Figs. 3 and 5 shows that dependences of $-RT\ln K$ on $(\Delta r/d)^2$ and E_{ds} on $(\Delta r/d)^2$ are expectedly related, i.e., K values decrease with increasing E_{ds}. Heterovalent impurities have low K and high E_{ds} values, even at small size difference with respect to the substituted ion. Dependences of $-RT\ln K$ on $(\Delta r/d)^2$ significantly deviate from the origin, which may be caused to a large degree by energy consumption for the formation of charge compensator. It was experimentally established [54] that in the case of coupled isomorphism of Cr^{3+} and Li^+, K_{Cr} increases by one and a half times and K_{Li}, by two times, which corresponds to a decrease of calculated E_{ds} by 140 kJ/mol for Cr^{3+} and by 160 kJ/mol for Li^+. This also indicates a strong correlation between K and E_{ds}.

The linear dependence of $-RT\ln K$ on E_{ds} (Fig. 8) can be expressed by the following equations:

$$Me^{2+}: -RT\ln K = 1(0.2)E_{ds} + 30(8), \quad R^2 = 0.91;$$

$$Me^{3+}: -RT\ln K = 1.5(0.4)E_{ds} - 230(80), \quad R^2 = 0.82;$$

$$Me^{4+}: -RT\ln K = 0.15(0.05)E_{ds} + 50(14), \quad R^2 = 0.81.$$

The slope of these dependences increases in the following sequence $Me^{4+} < Me^{2+} < Me^{3+}$. The free term characterizing the deviation of the linear correlation from the origin does not exceed 50 kJ/mol for isovalent substitutions, whereas this deviation is large (>200 kJ/mol) to negative values for trivalent impurities. We can suggest that the calculated static energy of impurity dissolution (E_{ds}) is close to the enthalpy of impurity dissolution at crystallization temperature [4]. In this case, the free term corresponds to the contribution of the entropy component to the free energy of impurity dissolution. For heterovalent substitutions, the contribution of the entropy component significantly increases as compared to isovalent substitution, which is probably related to the formation of a compensation defect restoring the crystal electroneutrality.

ACKNOWLEDGMENTS

The study was supported by the Russian Foundation for Basic Research (project nos. 05-05-64721 and 05-02-16750) and Federal Program for Support of Leading Scientific Schools (NSh-1955.2003.5).

REFERENCES

1. V. S. Urusov, V. L. Tauson, and V. V. Akimov, *The Geochemistry of Solids* (GEOS, Moscow, 1997) [in Russian].
2. L. A. Nisel'son and A. G. Yaroshevskii, *Coefficients of Interphase Fractionation: Crystal–Liquid and Liquid–Vapor Equilibria* (Nauka, Moscow, 1992) [in Russian].
3. V. S. Urusov, "The Phenomenological Theory of Solid Solutions," EMU Notes Mineral. **3**, 121–153 (2001).
4. N. L. Allan, J. D. Blundy, J. A. Purton, *et al.*, "Trace Element Incorporation in Minerals and Melts," EMU Notes Mineral. **3**, 251–302 (2001).
5. J. A. Purton, J. D. Blundy, and N. L. Allan, "Computer Simulation of High-Temperature, Forsterite–Melt Partitioning," Am. Mineral. **85**, 1087–1091 (2000).
6. J. Barthel, E. Buhrig, and K. Hein, *Crystallization from Melts* (Deutscher Verlag für Grundstoffindustrie, Leipzig, 1983; Metallurgiya, Moscow, 1987).
7. N. Onuma, H. Higuchi, H. Wakita, and H. Nagasawa, "Trace Element Partition between Two Pyroxenes and the Host Lava," Earth Planet. Sci. Lett. **5**, 47–51 (1968).
8. B. B. Jensen, "Patterns of Trace Element Partitioning," Geochim. Cosmochim. Acta **37**, 2227–2242 (1973).
9. J. A. Philpotts, "The Law of Constant Rejection," Geochim. Cosmochim. Acta **42**, 909–920 (1978).
10. P. Beattie, "Systematics and Energetics of Trace Element Partitioning between Olivine and Silicate Melts: Implications for the Nature of Mineral/Melt Partitioning," Chem. Geol. **117**, 57–71 (1994).
11. V. B. Dudnikova, E. V. Zharikov, V. S. Urusov, *et al.*, "The Ion Radius and the Impurity Charge as Factors of a Coefficient of the Impurity Fractionation between For-

sterite Crystal and Its Melt," Mater. Elektron. Tekh., No. 2, 11–14 (2000).

12. V. S. Urusov, *The Theory of Isomorphism* (Nauka, Moscow, 1977) [in Russian].
13. J. D. Blundy and B. J. Wood, "Prediction of Crystal–Melt Partition Coefficients from Elastic Module," Nature **372**, 452–454 (1994).
14. B. J. Wood and J. D. Blundy, "A Predictive Model for Rare Earth Element Partitioning between Clinopyroxene and Anhydrous Silicate Melt," Contrib. Mineral. Petrol. **129**, 166–181 (1997).
15. J. D. Blundy, J. A. C. Robinson, and B. J. Wood, "Heavy REE Are Compatible in Clinopyroxene on the Spinel–Lherzolite Solidus," Earth Planet. Sci. Lett. **160**, 493–504 (1998).
16. J. D. Blundy and J. A. Dalton, "An Experimental Comparison of Clinopyroxene–Melt Partitioning in Silicate and Carbonate Systems and Implications for Mantle Metasomatism," Contrib. Mineral. Petrol. **139**, 356–371 (2000).
17. J. M. Brenan, H. F. Shaw, F. J. Ryerson, and D. L. Phinney, "Experimental Determination of Trace Element Partitioning between Pargasitic Amphibole and Synthetic Hydrous Melt," Earth Planet. Sci. Lett. **135**, 1–12 (1995).
18. T. LaTourette, R. L. Hervig, and J. R. Holloway, "Trace Element Partitioning between Amphibole, Phlogopite, and Basanite Melt," Earth Planet. Sci. Lett. **135**, 13–30 (1995).
19. P. Moller, "The Dependence of Partition Coefficients on Differences of Ionic Volumes in Crystal–Melt Systems," Contrib. Mineral. Petrol. **99**, 62–69 (1988).
20. V. B. Dudnikova, V. S. Urusov, A. B. Bykov, and G. M. Kolesov, "Fractionation of Trace Trivalent Admixtures between Forsterite and Melt," Geokhimiya, No. 3, 444–447 (1992).
21. R. D. Shannon, "Revised Effective Ionic Radii and Systematic Studies of Interatomic Distances in Halides and Chalcogenides," Acta Crystallogr. **A32**, 751–767 (1976).
22. V. B. Dudnikova, E. V. Zharikov, N. N. Eremin, *et al.*, "Vanadium Distribution between Forsterite and Its Melt: The Structural and Oxidation State of Vanadium," Geokhimiya, No. 7, 734–743 (2001) [Geochem. Int. **39** (7), 667–675 (2001)].
23. V. B. Dudnikova, A. V. Gaister, E. V. Zharikov, *et al.*, "Chromium Distribution between Forsterite and Its Melt: Dependence on Chromium Content in Melt and Redox Conditions," Geokhimiya, No. 5, 519–526 (2005) [Geochem. Int. **43** (5), 471–477 (2005)].
24. L. Shenjun, L. Lin, W. Zulun, J. Yandao, *et al.*, "Growth and Characteristics of Mg_2SiO_4: Ti Crystal," J. Cryst. Growth **139**, 327–331 (1994).
25. T. Kobayashi and H. Takei, "Distribution of Some Trivalent Ions between Melt and Single Crystals Mg_2SiO_4 Grown by Czochralski Method," Earth Planet. Sci. Lett. **36**, 231–236 (1977).
26. I. D. Birle, G. V. Gibbs, P. B. Moore, and J. V. Smith, "Crystal Structure of Natural Olivines," Am. Mineral. **53**, 807–825 (1968).
27. J. D. Gale, "GULP: A Computer Program for the Symmetry Adopted Simulation of Solids," J. Chem. Soc. Faraday Trans. **93**, 629–637 (1997).
28. C. M. Freeman and C. R. A. Catlow, "A Computer Modeling Study of Defect and Dopant States in SnO_2," J. Solid State Chem. **85**, 65–75 (1990).
29. G. V. Lewis and C. R. A. Catlow, "Potential Models for Ionic Oxides," J. Phys. Solid State Phys. **18**, 1149–1161 (1985).
30. M. J. Sanders, M. J. Leslie, and C. R. A. Catlow, "Interatomic Potentials for SiO_2," J. Chem. Soc. Chem. Com. **18**, 1271–1273 (1984).
31. R. M. Hazen, "Effects of Temperature and Pressure on the Crystal Structure of Forsterite," Am. Mineral. **61**, 1280–1293 (1976).
32. D. M. Smyth and R. L. Stocker, "Point Defect and Non-Stoichiometry in Forsterite," Phys. Earth Planet. Int. **10**, 183–192 (1975).
33. K. Andersson, G. Borchart, S. Scherrer, and S. Weber, "Self Diffusion in Mg_2SiO_4 (Forsterite) at High Temperature: A Model Case Study for SIMS Analyses on Ceramic Surfaces," Fresenius Z. Anal. Chem. **333**, 383–385 (1989).
34. O. Jaoul, Y. Bertran–Alvarez, R. C. Liebermann, and G. D. Price, "Fe–Mg Interdiffusion in Olivine up to 9 GPa at T = 600–900°C: Experimental Data and Comparison with Defect Calculations," Phys. Earth Planet. Int. **89**, 199–218 (1995).
35. J. A. Purton, N. L. Allan, J. D. Blundy, and E. A. Wasserman, "Isovalent Trace Element Partitioning between Minerals and Melts: A Computer Simulation Study," Geochim. Cosmochim. Acta **60**, 4977–4987 (1996).
36. J. A. Purton, N. L. Allan, and J. D. Blundy, "Calculation Solution Energies of Heterovalent Cations in Forsterite and Diopside: Implication for Trace Element Partitioning," Geochim. Cosmochim. Acta **61**, 3927–3936 (1997).
37. V. Rajamani, G. E. Brown, and C. T. Prewitt, "Cation Ordering in Ni–Mg Olivine," Am. Mineral. **60**, 292–299 (1975).
38. N. R. Khisina, S. S. Meshalkin, A. A. Borisov, and V. S. Urusov, *The Coefficient of Fe and Mg Intracrystal Distribution in Olivine as a Function of T and* f_{O_2}, Geokhimiya, No. 8, 1096–1107 (1990).
39. V. S. Urusov, I. V. Lapina, Yu. K. Kabalov, and I. F. Kravchuk, "Isomorphism in the Forsterite–Tephroite Series," Geokhimiya, No. 7, 1047–1055 (1984).
40. T. C. McCormick, J. R. Smyth, and G. E. Lofgren, "Site Occupancies of Minor Elements in Synthetic Olivines as Determined by Channeling-enhanced X-ray Emission," Phys. Chem. Miner. **14**, 368–372 (1987).
41. J. M. Gaite, "Pseudo-symmetries of Crystallographic Coordination Polyhedra: Application to Forsterite and Comparison with Some EPR Results," Phys. Chem. Miner. **6**, 9–17 (1980).
42. J. L. Mass, J. M. Burlitch, S. A. Markgraf, *et al.*, "Oxygen Activity Dependence of Chromium (IV) Population in Chromium-doped Forsterite Crystals Grown by Floating Zone Technique," J. Cryst. Growth **165**, 250–257 (1996).
43. H. Rager, "Electron Spin Resonance of Trivalent Chromium in Forsterite, Mg_2SiO_4," Phys. Chem. Miner. **1**, 371–378 (1977).

44. H. Rager, "Electron–Nuclear Hyperfine Interaction of $^{53}Cr^{3+}$ in Mg_2SiO_4 (Forsterite)," Z. Naturforsch., A: Phys. Sci. **35A**, 1296–1303 (1980).
45. D. E. Budil, D. G. Park, J. H. Freed, *et al.*, "9.6 GHz and 34 GHz Electron Paramagnetic Resonance Studies of Chromium-doped Forsterite," J. Chem. Phys. **101**, 3538–3548 (1994).
46. D. L. Anderson and O. L. Anderson, "The Bulk Modulus–Volume Relationship for Oxides," J. Geophys. Res. **75**, 3494–3500 (1970).
47. O. L. Anderson, "Patterns in Elastic Constants of Minerals Important to Geophysics," in *Nature of Solid Earth*, Ed. by E. C. Robinson (McGraw-Hill, New York, 1972), pp. 575–613.
48. E. V. Zharikov, V. Yu. Fedorovich, and V. F. Kitaeva, Preprint No. 4, FIAN (Phys. Inst. Russ. Acad. Sci., Moscow, 1980).
49. E. V. Zharikov and V. Yu. Fedorovich, Preprint No. 13, FIAN (Phys. Inst. Russ. Acad. Sci., Moscow, 1990).
50. R. M. Hazen and L. W. Finger, *Comparative Crystal Chemistry: Temperature–Pressure–Compression and Variation of Crystal Structure* (Wiley, New York, 1982).
51. V. S. Urusov and V. B. Dudnikova, "The Trace-component Trapping Effect: Experimental Evidence, Theoretical Interpretation, and Geochemical Applications," Geochim. Cosmochim. Acta **62** (7), 1233–1240 (1998).
52. R. O. Colson, G. A. McKay, and L. A. Taylor, "Temperature and Composition Dependencies of Trace Element Partitioning: Olivine/Melt and Low-Ca Pyroxene/Melt," Geochim. Cosmochim. Acta **52** (7), 539–553 (1988).
53. B. J. Wood and J. D. Blundy, "The Effect of Cation Charge on Crystal–Melt Partitioning of Trace Element," Geotektonika **188**, 59–71 (2001).
54. V. B. Dudnikova, A. V. Gaister, E. V. Zharikov, *et al.*, "The Coupled Isomorphism as a Factor of the Chromium Distribution in Forsterite," Neorgan. Mater. **39** (8), 985–990 (2003).